frontiers | Frontiers in Marine Science

TYPE Original Research
PUBLISHED 04 January 2024
DOI 10.3389/fmars.2023.1300005

Cyclic resistance evaluation of marine clay based on CPTu data: a case study of Shaba Wind Farm

Qi Wu[1], En-ci Zhu[1], Xing Xiao[1*], Yuan-xi Li[2] and Guo-xing Chen[1]

[1]Institute of Geotechnical Engineering, Nanjing Tech University, Nanjing, Jiangsu, China, [2]China Energy Engineering Group Guangdong Electric Power Design Institute Co., Ltd., Guangzhou, Guangdong, China

OPEN ACCESS

EDITED BY
Xingsen Guo,
University College London, United Kingdom

REVIEWED BY
Xiaotong Yang,
Tsinghua University, China
Xianwei Zhang,
Chinese Academy of Sciences (CAS), China
Zhongkun Ouyang,
Tsinghua University, China
Xiaotong Yang,
Tsinghua University, China in collaboration with reviewer ZO

*CORRESPONDENCE
Xing Xiao
xx_0524@126.com

RECEIVED 23 September 2023
ACCEPTED 05 December 2023
PUBLISHED 04 January 2024

CITATION
Wu Q, Zhu E-c, Xiao X, Li Y-x and Chen G-x (2024) Cyclic resistance evaluation of marine clay based on CPTu data: a case study of Shaba Wind Farm.
Front. Mar. Sci. 10:1300005.
doi: 10.3389/fmars.2023.1300005

The offshore wind farm industry has recently experienced significant global growth. This study presents a thorough site investigation and analysis of the cyclic resistance of marine clay for offshore foundation design, using the Shaba wind farm in southern China as a case study. *In-situ* cone penetrometer (CPTu) tests and borehole sampling are conducted to explore the geotechnical characteristics of the soils. However, the soil conditions are characterized by multiple layers and complex sedimentary components. The classification and mechanical properties, such as water content and cyclic resistances, are compared through CPTu interpretation and laboratory tests. The findings indicated that a single physical indicator cannot determine cyclic resistance. In addition, the well-established method in existing literature proved unsuitable for marine clay. Consequently, multiple regression analysis shows that a linear relationship exist between cyclic resistance and depth-corrected CPTu index $[EXP(q_E/f_s)^{0.3}/H]$, hence a new evaluation method is developed to predict the cyclic resistance of marine clay based on CPTu data. This research aims to provide more reliable guidance for geotechnical investigations, supporting the rapid expansion of offshore wind farms.

KEYWORDS
site investigation, CPTU, cyclic resistance, marine clay, offshore wind farms

1 Introduction

Wind energy, a sustainable and environmentally friendly energy source, offers an innovative path for global efforts in addressing energy shortages. The installed capacity of offshore wind turbines has shown consistent annual growth. These turbines are typically anchored to the seabed, often involving marine clay layers. Foundation costs, comprising approximately 25%–35% of total costs (Bhattacharya, 2014), necessitate various marine clay parameters for the geotechnical design of diverse foundation solutions. Under complex marine environmental loads, such as wind, waves, storms, and earthquakes, marine clay demonstrates notable stiffness degradation characteristics (Yang et al., 2018; Pan et al., 2021; Xiao et al., 2023) and can even lose strength entirely. Thus, understanding the cyclic resistance of marine clay is crucial for foundation design. However, its precise determination and rational design pose significant challenges in engineering construction (Lunne et al., 2006; Berre et al., 2022; Gao et al., 2024).

The predominant method to determine marine clay's cyclic resistance involves laboratory cyclic tests, including cyclic triaxial tests, cyclic torsional shear tests, and cyclic direct simple shear tests. These tests demand high-quality soil samples and skilled testers. Nevertheless, soil sample disturbance during drilling and transport can compromise the accuracy of these tests in representing marine clay's *in-situ* cyclic resistance. In addition, the requirement for a large volume of soil samples substantially increases the cost. Consequently, the engineering community urgently seeks effective methods to ascertain marine clay's cyclic resistance with fewer tests.

Comprehensive *in-situ* and laboratory tests are indispensable in acquiring site geotechnical properties and soil parameters. Cone penetrometer (CPTu) tests are preferred for *in-situ* testing due to their high accuracy, convenience, and speed (Cai et al., 2012; Cai et al., 2016; Duan et al., 2017; Meng and Pei, 2023). CPTu data comprehensively represent soil strength and deformation capacity under static and dynamic loading. Over the past decades, CPTu-based undrained shear strength evaluation methods for soils have been extensively developed (Sandven, 1990; Eslami, 1997). Subsequently, researchers began developing cyclic strength evaluation methods based on *in-situ* and laboratory tests (Olsen, 1994; Robertson and Wride, 1998; Robertson, 2009). Juang et al. (2008) developed a deterministic CPTu-based cyclic resistance evaluation method applicable to various soil types. Juang et al. (2012) and Ku and Juang (2012) refined this model. Notably, these models were formulated using CPTu data for terrestrial soils. However, marine clays, influenced by factors like high salt content, low-temperature seawater environments, unique cementitious materials, and complex hydrodynamics, develop flocculated structures distinct from terrestrial soils. Thus, terrestrial clay cyclic resistance models are not directly transferable to marine clays. Limited research focuses on evaluating marine clay cyclic resistance. He et al. (2021) and Wang et al. (2022) explored the cyclic behavior of marine soils using CPTu tests, but they did not develop predictive models. Therefore, creating and refining a cyclic resistance evaluation method for marine clay based on *in-situ* and laboratory tests is essential.

This study conducts a case study involving CPTu tests at the Shaba offshore wind farm in southern China to establish a cost-effective method to evaluate marine clay cyclic resistance. Soil stratigraphy is delineated, highlighting the soil's multilayered and complex sedimentation. In addition, consolidated undrained cyclic triaxial tests on marine clay are conducted to assess cyclic resistance, a vital parameter for foundation design. The well-established CPTu-based cyclic resistance evaluation methods in existing literature are not fully applicable to marine clays. Ultimately, this research develops a CPTu-based cyclic resistance evaluation method for marine clay at the Shaba offshore wind farm. The study's findings will offer assistance and guidance for constructing offshore wind farms in China.

2 Site description

The Yangjiang Shaba Offshore Wind Farm is situated in the southern sea area of Shaba Town, Yangxi County, Yangjiang City, Guangdong Province, as illustrated in Figure 1. This wind farm lies approximately 20 kilometers offshore. The area's sea is expansive, lacks islands, and features relatively flat terrain. Water depths vary

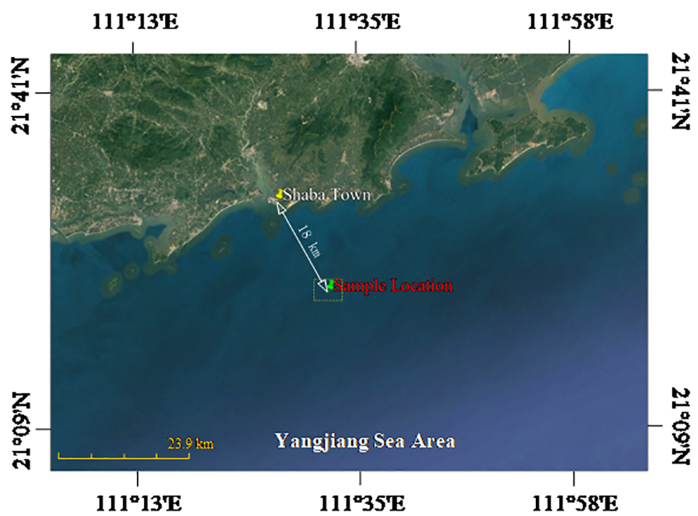

FIGURE 1
Site location (Base map data © 2023 Google).

from 23 to 27 meters, with an average tidal range of around 2.73 meters. Summer months bring significant typhoon impacts, leading to maximum wave heights near 8 meters.

The site is positioned at the Rudong River's mouth, where the sedimentary environment is notably complex, shaped by the combined influences of river flow and ocean waves. Sediments primarily comprise marine, alluvial marine, and residual deposits, characterized by a swift sedimentation rate. Soil stratification will be elaborated upon based on CPTu and borehole sampling results. In addition, the sea area at this location is spacious, devoid of surrounding islands. The seafloor topography is predominantly gentle, showing a trend of higher elevation in the northwest and lower in the southeast. No potential submarine geological hazards, such as underwater landslides, have been identified.

3 CPTu tests and soil characteristic

3.1 CPTu test results

This project entailed offshore field investigations, encompassing 4 CPTu tests (CPTu1, CPTu2, CPTu3, and CPTu4) and four borehole samplings (Y1, Y2, Y3, and Y4), with each borehole sampling site situated about 1 meter from its corresponding CPTu test hole. The CPTu tests utilized the ROSON seabed digital CPT penetration equipment by Van Den Berg, Netherlands. This device operates at a penetration speed of 20 mm/s, boasts a maximum thrust of 50 kN, and can penetrate up to 40 meters deep. It can perform continuous CPTu tests in seabeds with water depths reaching 1500 meters. Borehole sampling employed hydrostatic pressure-driven methodology. Standard Shelby tube samplers were used for soft clay, while thick-walled tube samplers were applied for silty mud and sandy soil. The depths of CPTu1, CPTu2, Y1, and Y2 are 14 meters; CPTu3 and Y3 are 24 meters deep; and CPTu4 and Y4 are 28 meters.

Figure 2 displays the CPTu test results for the four boreholes. Notable fluctuations in q_c (cone resistance), f_s (sleeve friction), and u_2 (pore water pressure) are evident with depth in each borehole, signifying multiple soil layers. Utilizing the CPTu data and laboratory test outcomes, the stratigraphic details of soil layers were determined following the ASTM D2487 (ASTM, 2017) standard. A simplified diagram representing this information accompanies the CPTu test results. Wu et al. (2023) comprehensively described soil stratification methods. The geological strata mainly consist of marine-terrestrial transitional sedimentary layers. The upper part includes Holocene marine deposits, encompassing sludge and medium sand mixed sludge. The lower part comprises the Holocene sea-land transitional sedimentary layer and the late Pleistocene sea-land alternating sedimentary layer, containing clay, silt, fine sand, medium sand, and coarse sand. This study focuses on clay; hence, emphasis is placed on CPTu data pertinent to clay layers. Compared to cohesionless soil and rock layers, the q_c and f_s values for clay layers are relatively low and show little depth dependence, while the u_2 values are higher and typically increase with depth. In addition,

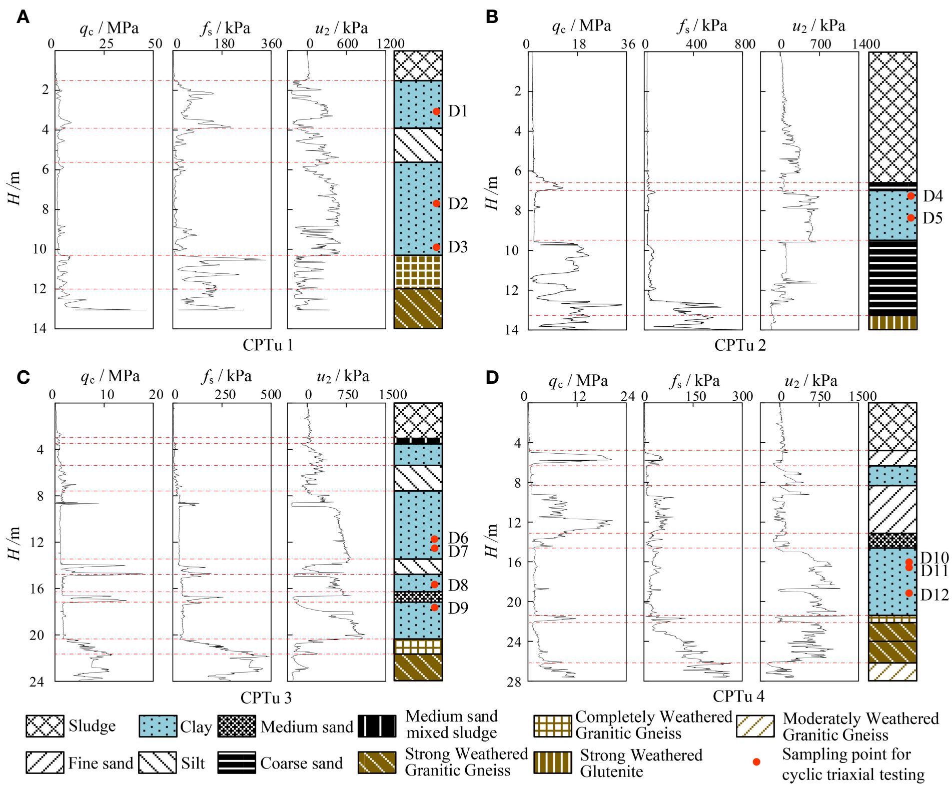

FIGURE 2
CPTu results and soil layer classifications. (A–D are four different boreholes).

an inverse relationship exists between u_2 and q_c, indicating that higher u_2 values correspond to lower q_c values. This aligns with the principles of effective stress.

3.2 Index properties of marine clay

The natural water content (w_0), density (ρ), plasticity index (I_p), and initial void ratio (e_0) of the clay samples (D1~D12, as shown in Figure 2) in the stratum were determined in accordance with ASTM D2216 (ASTM, 2019), D1556/D1556M (ASTM, 2015), and D4318 (ASTM, 2017), respectively. The results are depicted in Figure 3. The properties of the clay layers in the four boreholes exhibit considerable uniformity. The natural water content remains relatively consistent within each borehole, while I_p and ρ gradually increment with depth. Concurrently, e_0 exhibits a steady decrease with increasing depth. The red points in Figure 3 symbolize the samples utilized for conducting undrained cyclic triaxial tests. Table 1 summarizes their fundamental physical properties, whereas Figure 4 depicts their positions on the plasticity chart. These clays are categorized as CH and CL based on ASTM D2487 (ASTM, 2017).

4 Consolidated undrained triaxial test

4.1 Test program

The undrained cyclic triaxial tests were conducted using a dynamic triaxial system provided by GDS Instruments Ltd., UK. Chen et al. (2020) and Ma et al. (2023) offer more comprehensive details. Table 2 lists the primary technical specifications of the controller parameters, sensor range, accuracy, deviation, and other pertinent details. The following must be considered to conduct undisturbed marine clay cyclic triaxial tests following ASTM D5311 (ASTM, 2013): (1) Mold undisturbed marine clay samples into solid cylindrical specimens measuring 50 mm in diameter and 100 mm in height. (2) Situate the prepared specimens in a saturation vessel within a vacuum saturation chamber, initiating specimen saturation via the vacuum method (Lu et al., 2021). (3) Once vacuum saturation concludes, position the sample atop the pedestal in the dynamic triaxial system. (4) Implement backpressure saturation; after each stage, determine the B value, continuing until B exceeds 0.95, signifying complete saturation. (5) Apply uniform consolidation to the fully saturated specimen, selecting the confining pressure based on *in-situ* effective stresses. Based on ASTM D4767 (ASTM, 2020), consolidation is deemed complete when the average strain rate of the specimen falls below 1×10^{-3}%/min. Assessing sample quality or disturbance degree prior to laboratory testing is crucial. Lunne et al. (1997) index, assessing sample quality based on void ratio alterations due to loading relative to *in-situ* effective stresses, was employed in this study, as indicated in Table 1. The findings categorize all examined samples as either "very good to excellent" or "good to fair," with evaluation criteria detailed in Table 3.

Post-consolidation, sinusoidal wave loading at a frequency of 0.1 Hz is applied to the specimen. The specific test plan is listed in Table 1. Several tests involving three distinct cyclic stress ratio (CSR) levels are conducted on specimens sharing the same identification. As shown in Equation (1), the CSR is defined as follows:

$$CSR = \sigma_d / 2\sigma_{c0}^{'} \tag{1}$$

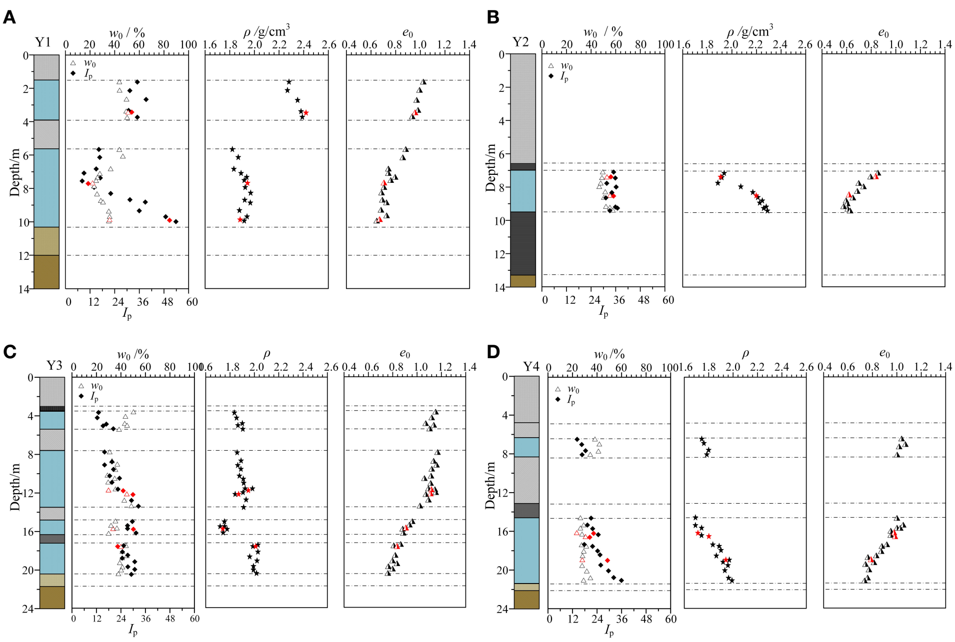

FIGURE 3
Index properties of marine clay versus depth. (**A–D** are four different boreholes).

TABLE 1 Basic physic properties and scheme of undisturbed marine clay.

Test number	Physical properties									Test scheme		
	H/m	ρ	w/%	w_L/%	I_p	e_0	e_c	$\Delta e/e_0$	Soil code	σ'_{c0}/kPa	CSR	N_f
D1-1	3.2-3.6	2.42	49.25	52.32	32.3	0.960	0.916	0.046	CH	50	0.12	341
D1-2							0.911	0.051			0.14	102
D1-3							0.923	0.039			0.15	40
D2-1	7.2-7.6	1.91	27.67	42.15	18.5	0.707	0.679	0.039	CL	50	0.15	114
D2-2							0.685	0.031			0.16	43
D2-3							0.688	0.027			0.18	26
D3-1	7.5-7.9	1.95	22.10	26.80	11.1	0.671	0.650	0.031	CL	50	0.3	237
D3-2							0.630	0.061			0.32	21
D3-3							0.638	0.049			0.33	6
D4-1	8.3-8.7	2.20	30.15	39.80	19.8	0.838	0.813	0.030	CL	55	0.35	423
D4-2							0.800	0.046			0.36	10
D4-3							0.788	0.060			0.38	3
D5-1	9.7-10.1	1.89	36.00	66.65	50.73	0.614	0.589	0.041	CH	65	0.16	585
D5-2							0.578	0.059			0.18	151
D5-3							0.594	0.033			0.19	82
D6-1	11.6-12.0	1.95	29.85	48.51	25.1	1.116	1.085	0.028	CL	80	0.13	1219
D6-2							1.075	0.037			0.15	473
D6-3							1.074	0.038			0.17	5
D7-1	12.0-12.4	1.87	44.85	51.55	29.9	1.119	1.068	0.046	CH	80	0.13	587
D7-2							1.062	0.051			0.15	87
D7-3							1.074	0.040			0.16	8
D8-1	15.6~16.0	1.74	33.60	53.64	30.1	0.908	0.876	0.035	CL	105	0.14	486
D8-2							0.875	0.036			0.16	18
D8-3							0.867	0.045			0.17	4
D9-1	16.0-16.4	1.71	23.54	47.99	22.4	0.836	0.803	0.039	CL	105	0.13	440
D9-2							0.796	0.048			0.14	215
D9-3							0.798	0.045			0.16	30
D10-1	16.4-16.8	1.80	30.74	43.35	20.5	0.981	0.920	0.062	CL	110	0.12	530
D10-2							0.929	0.053			0.15	90
D10-3							0.933	0.049			0.17	80
D11-1	17.2-17.6	2.01	40.00	46.58	22.4	0.984	0.945	0.039	CH	115	0.08	223
D11-2							0.934	0.050			0.11	26
D11-3							0.929	0.056			0.13	21
D12-1	18.8-19.2	1.94	28.10	52.36	29.2	0.788	0.754	0.043	CH	125	0.19	213
D12-2							0.735	0.067			0.23	40
D12-3							0.736	0.066			0.29	20

H is the depth below the seabed, ρ is the natural density, w is the natural water content, w_L is the liquid limit, I_p is the plasticity index, e_0 is the initial void ratio, e_c is the void ratio after consolidation, and N_f is the number of cycles to failure.

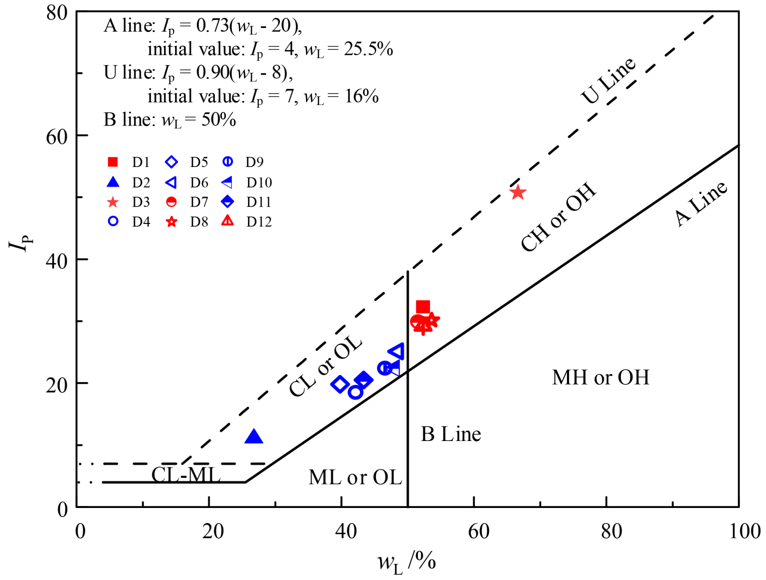

FIGURE 4
Soil classification lines.

where σ_d is the dynamic Stress Amplitude, σ'_{c0} is the initial effective consolidation stress.

4.2 Representative cyclic responses

Figure 5 displays typical results for the excess pore water pressure ratio r_u, axial strain (ϵ) curves, cyclic axial stress, deviator stress-axial strain curve, and effective stress path for D11-2. In these results, the excess pore water pressure ratio (r_u) is the ratio of excess pore pressure to initial confining stress. The double amplitude axial strain (ϵ_{DA}) is the difference between the maximum and minimum axial strains in each cycle. N_f is the number of cycles needed for the specimen to meet the failure criterion, with this criterion being ϵ_{DA} reaching 15% in this test. Figure 5A indicates that the development of ϵ exhibits progressive characteristics during the cyclic loading process. Initially, ϵ increases slowly in a linear manner. As the number of cyclic loading cycles N increases, ϵ grows rapidly, reaching the failure criterion after a relatively small number of cycles. Figure 5B shows that under cyclic loading, the rise in excess water pore pressure in the clay specimen is gradual, and it is challenging for r_u to increase to 1.0. At failure, r_u is only 0.48, attributed to the lower permeability of marine clay and the ongoing disruption of its cohesive structure due to cyclic loading. Figure 5C shows the relationship between the number of cycles and the axial stress. Figure 5D demonstrates that as N increases, the inclination of the hysteresis loop gradually diminishes, indicating a progressive decrease in the specimen's stiffness and strength. The shape evolves from "elliptical" to "Z" type. Concurrently, the vertical effective stress decreases, reflecting the development of pore water pressure during the cyclic process. The effective stress path shifts to the left with increasing cycle numbers, as shown in Figure 5E.

TABLE 2 The main technical specifications of the GDS dynamic triaxial test apparatus.

Sensor	Range	Deviation	Accuracy
Axial Force	5 kN	0.1% FS	0.2 N
Axial Displacement	± 50 mm	0.15% FS	0.2 μm
Axial Loading Frequency	≤ 2 Hz	–	–
Confining Pressure/ Back Pressure	2 MPa	0.15% FS	1 kPa
Confining Pressure/Back Pressure Volume	200 mm^3	0.25% FS	0.001 mm^3
Pore Water Pressure	2 MPa	0.15% FS	1 kPa

FS (Full Scale) = Maximum Range.

4.3 Cyclic resistance in laboratory tests

Ishihara et al. (1980) proposed using a power function to describe the relationship between CSR and N_f. The relationship Equation (2) is as follows:

$$CSR = a \cdot N_f^{-b} \tag{2}$$

where a and b are the fitting parameters.

Figure 6 depicts the relationship curve between the CSR and N_f of the clay samples from the Shaba wind farm, with a dashed line representing the fitting curve. The results indicated that as CSR increases, N_f decreases, demonstrating that the marine clay is more prone to damage under high cyclic loading conditions. However, the change pattern in cyclic resistance for each specimen remains unclear.

N_f directly correlates with the seismic moment. Based on Idriss and Boulanger (2008), an N_f of 15 typically corresponds to a seismic

TABLE 3 Criteria for evaluation of soil sample quality (Lunne et al., 1997).

OCR	Δe/e$_0$			
	Very good to excellent	Good to fair	Poor	Very poor
1-2	<0.04	0.04-0.07	0.07-0.14	>0.14
2-4	<0.03	0.03-0.05	0.05-0.10	>0.10

Δe is the change in void ratio reconsolidated to in-situ stress, and e_0 is the initial void ratio.

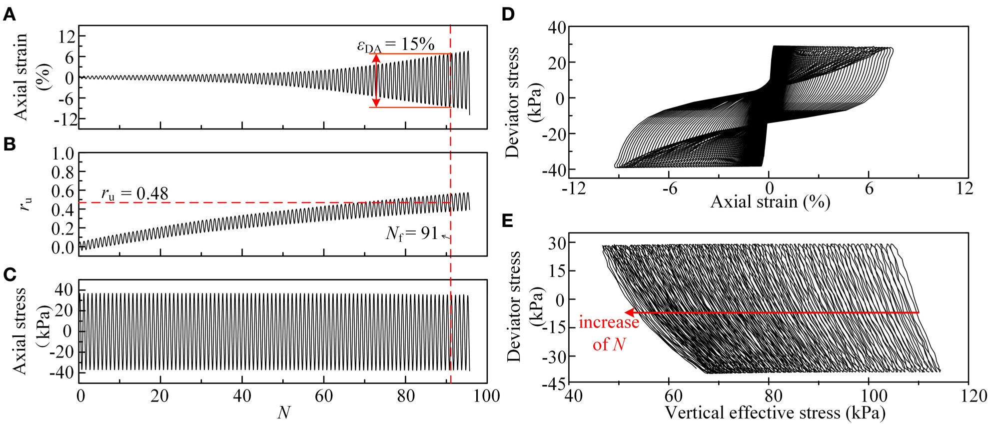

FIGURE 5
Undrained cyclic triaxial typical test results (**A–E** show five different typical test results).

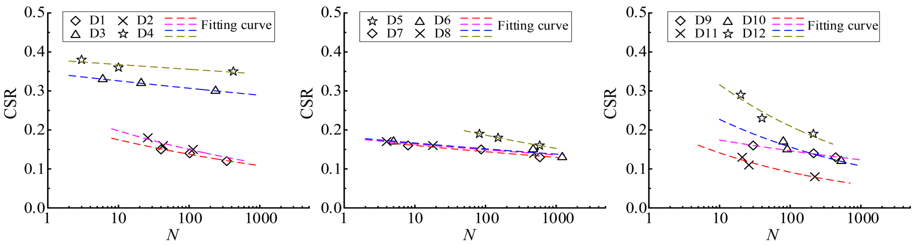

FIGURE 6
Dynamic strength curve of marine clay.

moment of 7.5. Hence, the *CSR* value corresponding to 15 cycles of uniform loading, extracted from the N_f vs. *CSR* correlation curve, represents its cyclic resistance (CRR_{lab}), as displayed in Table 4. Figure 7 illustrates the correlations between H, ρ, w, I_p, and CRR_{lab} of the tested sample. It indicates that CRR_{lab} does not significantly correlate with H, ρ, w, and I_p. Thus, it cannot evaluate CRR_{lab} by a single physical index of marine clay.

5 CPTu-based evaluation method for cyclic resistance of marine clay

Considering cone resistance as an indicator of the failure strength of soils *in situ* (Yu, 2006) and sleeve friction f_s as a measure of soil strength post-failure, Robertson and Wride (1998) proposed a complex cyclic resistance evaluation method. This approach considers *in-situ* vertical stress, soil behavior type index I_c, and modified cone resistance q_{t1N}. Juang et al. (2008) simplified the parameters and developed a method using the soil behavior type index $I_{c,BJ}$ and modified cone resistance q_{t1N}. Compared to Robertson and Wride's model, Juang et al.'s approach accounts for the influence of excess pore water pressure, offering insights into soil consolidation and permeability properties (Chai et al., 2011). In contrast, Olsen's method (Olsen, 1994) does not consider soil type and excess pore water pressure. These three models, based on CPTu tests on terrestrial soils, are summarized in Table 5. Figure 8 presents the field cyclic resistance ratio (CRR_{field}) calculated using these three models for four borehole locations. It reveals generally consistent trends in results calculated by each model with depth, albeit with notable differences in numerical values. At borehole locations CPTu

TABLE 4 Cyclic resistance of marine clay.

Test number	D1	D2	D3	D4	D5	D6	D7	D8	D9	D10	D11	D12
CRR_{lab}	0.161	0.185	0.322	0.366	0.204	0.164	0.157	0.161	0.166	0.177	0.120	0.267

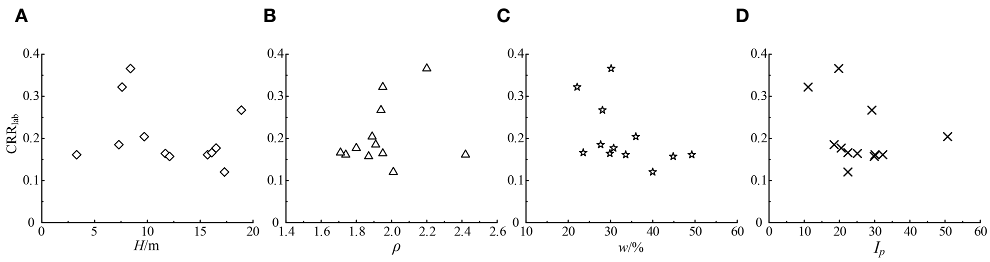

FIGURE 7
Correlation between H, ρ, w, I_p, and CRR_{lab}. (**A–D** are four different factors).

TABLE 5 CRR_{field} calculation model based on CPTu.

Reference	Empirical formula	Note
Robertson and Wride (1998)	$CRR_{field} = 93\left(\frac{q_{t1N,cs}}{1000}\right)^3 + 0.08, (50 \le q_{t1N,cs} < 160)$ $CRR_{field} = 0.833\left(\frac{q_{t1N,cs}}{1000}\right) + 0.05, (q_{t1N,cs} < 50)$	σ_{vo} = *in-situ* total vertical stress. σ'_{vo} = *in-situ* effective vertical stress. n = stress exponent. p_a = atmospheric pressure. q_{t1N} = modified cone resistance q_t = total cone resistance Q_{tn}, $q_{t1N,cs}$, F_r = cone parameters. f_s = sleeve friction. I_c = soil behavior type index. K_c is a function of I_c.
	$q_{t1N,cs} = K_c q_{t1N}$	
	$K_c = 1.0, I_c \le 1.64$ $K_c = -0.403I_c^2 + 5.58I_c^3 - 21.63I_c^2 + 33.75I_c - 17.88$	
	$q_{t1N} = \left(\frac{q_t - \sigma_{v0}}{P_a}\right) \times \left(\frac{P_a}{\sigma'_{v0}}\right)^n$	
	$n = 0.381I_c + 0.05(\sigma'_{v0}/P_a) - 0.15 \le 1.0$	
	$I_c = \sqrt{(3.47 - \lg Q_{tn})^2 + (1.22 + F_r)^2}$	
	$Q_{tn} = [(q_c - \sigma_{v0})/P_a]\left[(P_a/\sigma'_{v0})^n\right]$	
	$F_r = [f_s/(q_c - \sigma_{v0})] \times 100\,\%$	
Juang et al. (2008)	$CRR_{field} = 0.05 + \exp[A + B \times (q_{t1N}/100)^C]$	A、B、C = fitting parameter. $I_{c,BJ}$ = soil behaviour type index. q_c = modified cone resistance. Q_t, q_{c1}, F_r = cone parameters. B_q = excess pore pressure ratio.
	$A = I_{c,BJ}(q_{t1N}/100) - 14.7$	
	$B = 0.909I_{c,BJ}^3 - 7.47I_{c,BJ} + 19.28$	
	$C = 0.059 + 0.015I_{c,BJ}^2$	
	$I_{c,BJ} \sqrt{\{3 - \lg[Q_t(1 - B_q) + 1]\}^2 + [1.5 + 1.3(\lg F_r)]^2}$ $B_q = \frac{u_2 - u_0}{q_t - \sigma_{v0}}$	
Olsen (1994)	$CRR_{field} = 0.00128q_{c1} - 0.025 + 0.17R_f - 0.02R_f^2 + 0.0016R_f^3$	R_f = friction ratio. q_c = modified cone resistance.
	$q_{c1} = \frac{q_c}{(\sigma'_{v0})^{0.7}}$	

1, CPTu 3, and CPTu 4, Olsen's model yields the highest $CRR_{field,}$ followed by the Robertson model, with Juang's model providing the lowest values. In contrast, at borehole locations CPTu 2, Olsen's model results in the lowest CRRfield, Juang's model is intermediate, and the Robertson model calculates the highest values.

The laboratory test conditions are a simplified representation of field conditions. Differences often arise when applying results from laboratory cyclic triaxial tests to field situations. Seed (1979) proposed a conversion factor, C_r, to modify CRR_{lab}, yielding $CRR_{field,}$ as demonstrated in the subsequent Equation (3):

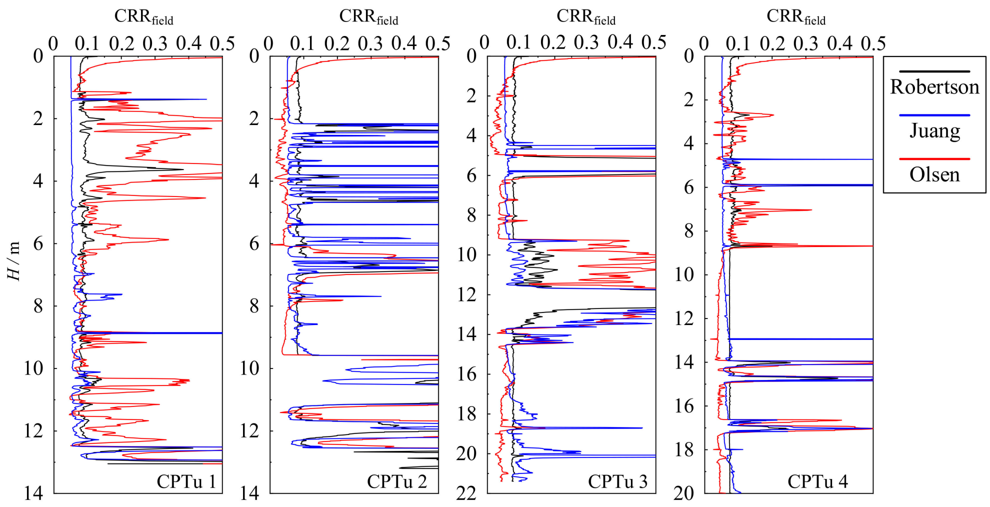

FIGURE 8
CRR_{field} calculation curve based on CPTu data.

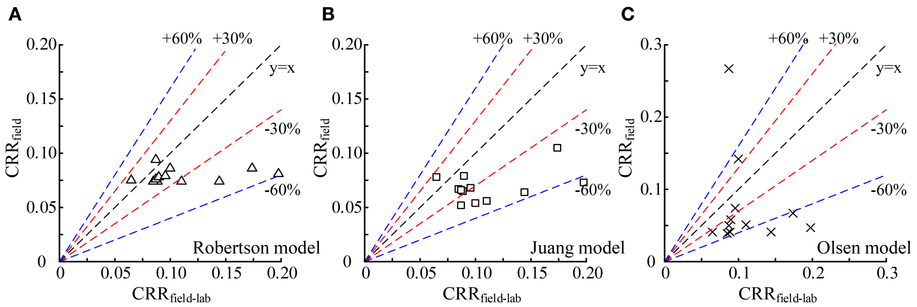

FIGURE 9
Comparison of CPTu-based CRR_{field} calculation results with indoor results CRR_{lab}. (**A–C** are three different methods).

$$CRR_{field-lab} = 0.9 \cdot C_r \cdot CRR_{lab} \tag{3}$$

where 0.9 is the correction factor for converting the laboratory cyclic resistance ratio under unidirectional loading to the cyclic resistance ratio under multiple-direction loading conditions in the field, C_r is taken as 0.7.

Comparisons of CRR_{field}, as calculated by various models at respective depths, with $CRR_{\text{field-lab}}$ determined by the test results are depicted in Figure 9. This figure reveals that Robertson's and Juang's approaches exhibit comparable effectiveness, with most errors remaining under 30% relative to $CRR_{\text{field-lab}}$. However, Olsen's method, which does not account for soil type and excess pore water pressure, shows the least accuracy, with errors surpassing 60%.

Accordingly, while CRR_{field} models derived from CPTu data show some applicability, the overall errors are significant. In addition, these models lack a clear functional relationship, potentially limiting their utility in practical engineering projects. As detailed in Section 3, the geotechnical properties of soil layers vary considerably at different depths. Incorporating soil characteristics indicated by q_t, u_2, and fs, and amalgamating laboratory test outcomes with CPTu data, a discernible functional relationship emerges among the effective cone tip resistance q_E (= q_t − u_2), f_s, and $CRR_{\text{field-lab}}$. Thus, an empirical model to predict CRRfield-lab for marine clay was formulated, using q_E, f_s, and H as independent variables, with $CRR_{\text{field-lab}}$ as the dependent variable, as delineated in Equation 4. Notably, H accounts for the *in-situ* stress of soils. Through multiple regression analysis, a new $CRR_{\text{field-lab}}$ evaluation method based on depth-corrected CPTu index $[EXP(q_E/f_s)^{0.3}/H]$ was developed, as Equation (4) shown, and its application to assess $CRR_{\text{field-lab}}$ for marine clay in the Yangjiang Wind Farm offshore area has demonstrated a robust fit, as illustrated in Figure 10.

$$CRR_{field-lab} = 0.018 + \frac{0.103 e^{(q_E/f_s)^{0.3}}}{H} \tag{4}$$

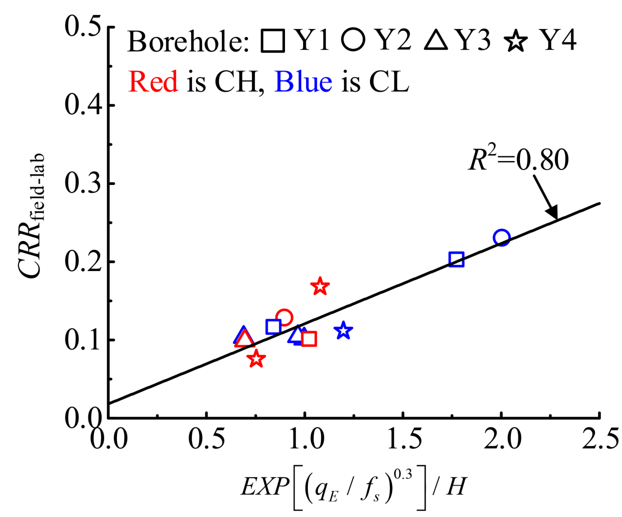

FIGURE 10
Dynamic strength evaluation method of marine clay based on CPTu data.

Noted that the CPTu-based $CRR_{\text{field-lab}}$ prediction model proposed in this study can effectively predict the cyclic resistance of marine clay, which makes up for the difficulty of sampling and high testing costs in offshore engineering. Also, compared with the above three well-developed prediction models (Olsen, 1994; Robertson and Wride, 1998; Juang et al., 2008), the $CRR_{\text{field-lab}}$ prediction model contains just only fewer basial physical parameters, i.e., if the depth H and CPTu data of marine clay are determined, then the $CRR_{\text{field-lab}}$ can be evaluated quickly and efficiently, which provides a significant advantage in the evaluation of liquefaction triggering of marine soils in practice.

6 Conclusion

This study presents the site investigation and cyclic resistance of marine clay, utilizing CPTu tests and advanced laboratory tests, taking the Shaba wind farm in southern China as a case study. An evaluation method for the cyclic resistance of marine clay, grounded in CPTu data, is introduced. The key conclusions are as follows:

1. The interpretation of CPTU data and index parameter tests depict the site conditions as having a multilayered and intricate sedimentary structure. The initial void ratio of clay layers shows a gradual increase with depth.
2. Under cyclic loading, the marine clay's hysteresis loop dip angle in the Yangjiang Sea region diminishes progressively, gradually reducing soil stiffness and strength. Concurrently, the maximum strain typically occurs post-peak stress, highlighting the delayed response between stress and strain in marine clay. In addition, the hysteresis curve's expansion toward the stretching direction suggests an elevated risk of tensile failure in the sample.
3. The CRR_{lab}, derived from consolidated undrained cyclic triaxial tests, was converted to an *in-situ* $CRR_{\text{field-lab}}$. Notable discrepancies were observed between the calculated results of the existing prediction methods based on CPTu data and the actual $CRR_{\text{field-lab}}$. Utilizing the CPTu data q_E, f_s, and depth H, a linear relationship existed between cyclic resistance and depth-corrected CPTu index $[EXP(q_E/f_s)^{0.3}/H]$. Then an alternative evaluation method to determine the $CRR_{\text{field-lab}}$ of marine clay was proposed. This method yielded prediction results that align well with engineering practice requirements.

Data availability statement

The raw data supporting the conclusions of this article will be made available by the authors, without undue reservation.

Author contributions

QW: Conceptualization, Data curation, Project administration, Resources, Validation, Visualization, Writing – original draft, Writing – review & editing. EZ: Data curation, Investigation, Methodology, Validation, Writing – original draft, Writing – review & editing. XX: Data curation, Investigation, Methodology, Validation, Visualization, Writing – review & editing. YL: Conceptualization, Methodology, Resources, Supervision, Validation, Visualization, Writing – review & editing. GC: Conceptualization, Data curation, Funding acquisition, Supervision, Validation, Visualization, Writing – review & editing.

Funding

The author(s) declare that no financial support was received for the research, authorship, and/or publication of this article.

Conflict of interest

Author YX-L was employed by China Energy Engineering Group Guangdong Electric Power Design Institute Co., Ltd.

The remaining authors declare that the research was conducted in the absence of any commercial or financial relationships that could be construed as a potential conflict of interest.

References

ASTM D1556/D1556M-15E01 (2015). *Standard test method for density and unit weight of soil in place by sand-cone method* (West Conshohocken, PA: ASTM International). doi: 10.1520/D1556_D1556M-15E01

ASTM D2216-19 (2019). *Standard test method for laboratory determination of water (moisture) content of soil and rock by mass* (West Conshohocken, PA: International). doi: 10.1520/D2216-19

ASTM D2487-17E01 (2017). *Standard practice for classification of soils for engineering purposes (Unified Soil Classification System)* (West Conshohocken, PA: ASTM International). doi: 10.1520/D2487-17E01

ASTM D4318-17E01 (2017). *Standard test method for sand content by volume of bentonitic slurries* (West Conshohocken, PA: ASTM International). doi: 10.1520/D4318-17E01

ASTM D4767-11 (2020). *Standard Test Method for Consolidated Undrained Triaxial Compression Test for Cohesive Soils* (West Conshohocken, PA: ASTM International). doi: 10.1520/D4767-11

ASTM D5311-13 (2013). *Standard test method for load controlled cyclic triaxial strength of soil* (West Conshohocken, PA: ASTM International). doi: 10.1520/D5311_D5311M-13

Berre, T., Lunne, T., and L'Heureux, J. S. (2022). Quantification of sample disturbance for soft, lightly overconsolidated, sensitive clay samples. *Can. Geotechnical J.* 2), 59. doi: 10.1139/cgj-2020-0551

Bhattacharya, S. (2014). Challenges in design of foundations for offshore wind turbines. *Eng. Technol. Ref. 0041* 1 (1), 922. doi: 10.1049/etr.2014.0041

Cai, G. J., Chu, Y., Liu, S. Y., and Puppala, A. J. (2016). Evaluation of subsurface spatial variability in site characterization based on RCPTU data. *Bull. Eng. Geology Environ.* 1), 1–12. doi: 10.1007/s10064-015-0727-8

Cai, G. J., Liu, S. Y., and Puppala, A. J. (2012). Reliability assessment of CPTU-based pile capacity predictions in soft clay deposits. *Eng. Geology* 141-142, 84–91. doi: 10.1016/j.enggeo.2012.05.006

Chai, J. C., Agung, P. M. A., Hino, T., Igaya, Y., and Cater, J. P. (2011). Estimating hydraulic conductivity from piezocone soundings. *Géotechnique* 61 (8), 699–708. doi: 10.1680/geot.10.P.009

Chen, G. X., Wu, Q., Zhao, K., and Shen, Z. F. (2020). A binary packing material-based procedure for evaluating soil liquefaction triggering during earthquakes. *J. Geotech Geoenviron. Eng.* 146 (6), 04020040. doi: 10.1061/(ASCE)GT.1943-5606.0002263

Duan, W., Liu, S. Y., and Cai, G. J. (2017). Evaluation of engineering characteristics of Lian-Yan railway soft soil based on CPTU data-A case study. *Proc. Eng.* 189, 33–39. doi: 10.1016/j.proeng.2017.05.006

Eslami, A. (1997). *Bearing capacity of piles from cone penetration test data* (Canada: University of Ottawa).

Gao, H., Sun, J., Stuedlein, A. W., Li, S., Wang, Z., Liu, L., et al. (2024). Flowability of saturated sands under cyclic loading and the viscous fluid flow failure criterion for liquefaction triggering. *J. Geotech Geoenviron. Eng.* 150 (1), 04023130. doi: 10.1061/JGGEFK.GTENG-11872

He, B., Yang, S. L., and Andersen, K. H. (2021). Soil parameters for offshore wind farm foundation design: A case study of Zhuanghe wind farm. *Eng. Geology* 285, 106055. doi: 10.1016/j.enggeo.2021.106055

Idriss, I. M., and Boulanger, R. W. (2008). *Soil liquefaction during earthquakes* (Earthquake Engineering Research Institute).

Ishihara, K., Troncoso, J., Kawase, Y., and Takahashi, Y. (1980). Cyclic strength characteristics of tailings materials. *Soils Found.* 20, 127–142. doi: 10.3208/sandf1972.20.4_127

Juang, C. H., Ching, J., Ku, C. S., and Hsieh, Y. H. (2012). Unified CPTu-based probabilistic model for assessing probability of liquefaction of sand and clay. *Géotechnique* 62 (10), 877–892. doi: 10.1680/geot.9.P.025

Juang, C. H., Chen, C. H., and Mayne, P. W. (2008). CPTU simplified stress-based model for evaluation soil liquefaction potential. *Soils Found* 48 (6), 755–770. doi: 10.3208/sandf.48.755

Ku, C. S., and Juang, C. H. (2012). "Liquefaction and cyclic softening potential of soils – a unified piezocone penetration testing-based approach," in *Géotechnique*. 62 (5), 457–461. doi: 10.1680/geot.10.P.044

Lu, X. F., Zhang, F., Qin, W. J., Zheng, H., and Feng, D. C. (2021). Experimental investigation on frost heave characteristics of saturated clay soil under different stress levels and temperature gradients. *Cold Reg. Sci. Tech* 192, 103379. doi: 10.1016/j.coldregions.2021.103379

Lunne, T., Berre, T., Andersen, K. H., Strandvik, S., and Sjursen, M. (2006). Effects of sample disturbance and consolidation procedures on measured shear strength of soft marine Norwegian clay. *Can. Geotech. J.* 43 (7), 726–750. doi: 10.1139/t06-040

Lunne, T., Berre, T., and Strandvik, S. (1997). Sample disturbance effects in soft low plastic Norwegian clay[C]//Symposium on Recent Developments in Soil and Pavement MechanicsCAPES-Fundacao Coordenacao do Aperfeicoamento de Pessoal de Nivel Superior; CNPq-Conselho Nacional de Desenvolvimento Cientifico a Tecnologico; FAPERJ-Fundacao de Ampora a Pesquisa do Estado do Rio de Janeiro; FINEP-Financiadora de Estudos e Projetos. Balkema, Rotterdam. 81–102.

Ma, W. J., Qin, Y., Wu, Q., Zhang, G. K., and Chen, G. X. (2023). Cyclic failure mechanisms of saturated marine coral sand under various consolidations. *Appl. Ocean Res.* 131, 103450. doi: 10.1016/j.apor.2022.103450

Meng, F. H., and Pei, H. F. (2023). Quasi-site-specific prediction of shear wave velocity from CPTu. *Soil Dynamics Earthquake Eng.* 172, 108005. doi: 10.1016/j.soildyn.2023.108005

Olsen, R. S. (1994). *Normalization and prediction of geotechnical properties using the cone penetrometer test (CPT)* (Berkeley: University of California).

Pan, K., Yuan, Z. H., Zhao, C. F., Tong, J. H., and Yang, Z. X. (2021). Undrained shear and stiffness degradation of intact marine clay under monotonic and cyclic loading. *Eng. Geol.* 297, 106502. doi: 10.1016/j.enggeo.2021.106502

Robertson, P. K. (2009). *Performance based earthquake design using the CPT* (Proc. IS-Tokyo), 3–20.

Robertson, P. K., and Wride, C. E. (1998). Evaluating cyclic liquefaction potential using the cone penetration test. *Can. geotechnical J.* 35 (3), 442–459. doi: 10.1139/t98-017

Sandven, R. B. (1990). *Strength and deformation properties of fine-grained soils obtained from piezocone tests* (Norway: Universitetet i Trondheim).

Seed, H. B. (1979). Soil liquefaction and cyclic mobility evaluation for level ground during earthquakes. *J. Geotechnical Eng. Division* 105 (2), 201–255. doi: 10.1061/AJGEB6.0000768

Wang, Y., Zhang, S. X., Xu, H., Zhang, Y. H., Gaunt, P., Ren, B., et al. (2022). Site investigation and soil parameters for offshore suction bucket design: A case study of Houhu wind turbine. *Ocean Eng.* 255, 111458. doi: 10.1016/j.oceaneng.2022.111458

Wu, Q., Zhu, E. C., H., L., Y., L., H., W., and Chen, G. X. (2023). A new empirical model for the undrained shear strength of undisturbed marine fine-grained soil based on piezocone penetration tests. *Appl. Ocean Res.* 141, 103770. doi: 10.1016/j.apor.2023.103770

Xiao, X., Hang, T. Z., Cai, Z. Y., Zhang, L., Wu, Q., and Chen, G. X. (2023). Cyclic threshold shear strain for pore water pressure generation and stiffness degradation in marine clays at Yangtze estuary. *Front. Mar. Sci.* 10. doi: 10.3389/fmars.2023.1184225

Yang, Q., Ren, Y. B., Niu, J. L., Cheng, K., Hu, Y. X., and Wang, Y. (2018). Characteristics of soft marine clay under cyclic loading: a review. *B. Eng. Geol. Environ.* 77 (3), 1027–1046. doi: 10.1007/s10064-017-1078-4

Yu, H. S. (2006). The First James K. Mitchell Lecture *In situ* soil testing: from mechanics to interpretation. *Geomechanics Geoengineering: Int. J.* 1-3, 165–195. doi: 10.1080/17486020600986884

Glossary

q_c	cone resistance
f_s	sleeve friction
u_2	pore water pressure
w_0	natural water content
ρ	natural density
I_p	plasticity index
e_0	initial void ratio
w_L	liquid limit
e_c	void ratio after consolidation
N_f	number of cycles to failure
r_u	excess pore water pressure ratio
ϵ_{DA}	double amplitude axial strain
CRR_{lab}	laboratory cyclic resistance
CRR_{field}	field cyclic resistance
$CRR_{field\text{-}lab}$	CRR_{lab} based on field correction
q_E	effective cone tip resistance
C_r	correction factor
N	number of cyclic loading cycles
σ'_{c0}	initial effective confining pressure
ϵ	axial strain
Δe	change of void ratio before and after consolidation
a, b	fitting parameters
CSR	cyclic stress ratio